Variable Damping Control for pHRI: Considering Stability, Agility, and Human Effort in Controlling Human Interactive Robots

Fatemeh Zahedi†, James Arnold†, Connor Phillips, and Hyunglae Lee*, *Member, IEEE*

***Abstract*—This paper presents a multi-degree-of-freedom variable damping controller to manage the trade-off between stability and agility and to reduce user effort in physical human-robot interaction. The controller accounts for the human body's inherent impedance properties and applies a range of robotic damping from negative (energy injection) to positive (energy dissipation) values based on the user's intent of motion. To evaluate the effectiveness of the proposed controller in balancing the trade-off between stability/agility and reducing user effort, two studies were performed on both the human upper-extremity and lower-extremity to represent both industrial and rehabilitation applications of the proposed controller. These studies required subjects to perform a series of multi-dimensional target reaching tasks while the human user interacted with either the end-effector of a robotic arm for the upper-extremity study or with a wearable ankle robot for the lower-extremity study. Stability, agility, and user effort were quantified by a variety of performance metrics. Stability was quantified by both overshoot and stabilization time. Mean and maximum speed were used to quantify agility. To quantify the user effort, both overall and maximum muscle activation, and mean and maximum root-mean-squared interaction force were calculated. The results of both the upper- and lower-extremity studies demonstrated that the controller was able to reduce user effort while increasing agility at a negligible cost to stability.**

***Index Terms*—Physical human robot interaction, variable impedance control, performance, stability, agility, human effort**

I. Introduction

THE field of physical human-robot interaction (pHRI) has steadily grown in recent years with new developments in a variety of applications. Human-robot systems for rehabilitation have allowed for enhanced physical therapy and powered prosthesis [1, 2], and industrial and military human-in-the-loop robots have seen increased development and design considerations [3–5].

To ensure system stability and safety of human-robot systems, researchers have designed and used different types of controllers [6–8]. One popular approach is impedance/admittance control which regulates the force/torque and displacement/angular displacement relationship at the interaction point [9, 10]. Such strategies often focus on using controllers that avoid adding energy into the system, often with highly dissipative behavior [11, 12]. One drawback of this approach is the additional effort required from the human user to overcome the dissipative behavior of the robot, which greatly reduces the performance of coupled human-robot systems in terms of agility and user effort. While these approaches can guarantee stability [13–15], they are not always desirable in circumstances where the robot is intended to increase the performance of the human within the coupled system. Therefore, the trade-off between stability and performance needs to be considered in controller design [11, 12].

The study of balancing the stability/agility tradeoff in pHRI is an active research field [16]. One approach used to address this problem was an impedance compensator based on the estimation of human joint/limb impedance [17]. However, this research was limited to movement along one axis. In another approach, a method was developed that detected increases in oscillation and acted to restore a stable behavior [18]. However, this method is highly task-dependent and requires knowledge about the human task and the corresponding parameter tuning. A less task-dependent approach is to define some metrics to quantify the intent of the user throughout the task such as change in velocity or force at the interaction point to alter robotic impedance parameters accordingly [19, 20]. This approach is versatile, but the inherent impedance of the human in the coupled system is not considered in these studies.

While the aforementioned research only focused on agility, a limited amount of other research has been focused on reducing user effort through impedance/admittance-based control [21–23]. The key idea of these works is to change the parameters of the impedance/admittance controller to ensure compliant motion. Although these approaches were successful in reducing user effort with guaranteed stability, they are either application-based approaches or costly regarding hardware design.

† These two authors contributed equally to this work.

Research supported by National Science Foundation Awards #1846885 and #1925110.

Fatemeh Zahedi, James Arnold, and Connor Phillips are with the School for Engineering of Matter, Transport and Energy, Arizona State University, Tempe, AZ 85287, USA (e-mail: {fzahedi1, jmarnol6, cmphil13}@asu.edu).

Hyunglae Lee is with the School for Engineering of Matter, Transport and Energy, Arizona State University, Tempe, AZ 85287, USA (e-mail: hyunglae.lee@asu.edu; *corresponding author: 480-727-7463; fax: 480-727-9321).

Previous research has been focused on either balancing the trade-off between agility/stability or reducing user effort, but, typically, both goals are equally important for pHRI applications. Therefore, this paper aims to quantify the stability, agility, and user effort in the evaluation of the proposed controller, namely a variable damping controller. This controller takes into account the inherent human impedance properties, in particular, human joint/limb damping, known from previous characterization studies [24–26] in order to design a controller that considers the summation of the damping contributions of both the robot and human within the coupled system.

With the knowledge that many limbs and joints in the human body are inherently positively damped, the variable damping controller can safely use negative robotic damping to inject energy into the system, while maintaining an overall stable human-robot system. The controller was developed on the principle that negative damping provides the user with agility while positive damping maintains stability [10, 17]. If the intent of the user can inform the damping behavior of the robot, then the robot can inject or dissipate energy from the system to minimize user effort and increase the agility without compromising stability of the coupled human-robot system. We hypothesized that the variable damping controller with the ability to quickly transition between negative and positive damping could achieve both stability and agility simultaneously, while reducing user effort.

To validate our hypothesis, we performed two distinct experiments simulating two different pHRI applications: 1) an industrial application using an upper-extremity robot, and 2) a rehabilitation application using a lower-extremity robot. For the upper-extremity study, we performed a set of human experiments that required subjects to interact with the end-effector of a 7 degree-of-freedom (DOF) robotic arm. For the lower-extremity study, human experiments were performed using a 2-DOF wearable ankle robot in a seated task. These two separate experiments allowed us to demonstrate the general applicability of the controller to different parts of the human body and different applications.

Our preliminary studies considered a one-dimensional (1D) version of the variable damping controller [27, 28]. These previous studies demonstrated that the variable damping control approach could improve the trade-off between stability and agility for simple, single plane tasks. However, most human movements in daily activities are more complex and involve movement in a multi-dimensional space. In this study, we introduce a 2D variable damping controller that more closely resembles what is necessary for real-world pHRI applications. Subjects completed a series of point-to-point target reaching tasks under constant positive damping and variable damping conditions. Stability, agility, and user effort were quantified by a variety of performance metrics that are used to demonstrate the general applicability of the controller for balancing the stability/agility trade-off and reducing the user effort.

II. Variable Damping Controller

A. Controller Description

The central goal of the proposed variable damping controller is to use the kinematic data collected by the robot to transition between negative (energy injecting) and positive (energy dissipating) damping. The kinematic information from the robot must be used to determine the user's intent of motion. In a typical target reaching task of a human extremity, the human will move their extremity in a predictable way: accelerate towards the target initially, then decelerate when they are nearing the desired target. During the initial acceleration phase of this movement, it is desirable for the robot to inject energy into the system, which can be realized through negative robotic damping. By applying negative damping, the robot is making it easier for the human user to move in the desired direction. By taking into account the magnitude of positive damping that is inherent in the human's extremity, the robot will be able to prevent the coupled human-robot system from becoming unstable. As long as the magnitude of the negative damping provided by the robot is less than the magnitude of the positive damping inherent in the extremity, the coupled system will remain stable despite the injection of energy by the robot. As the human user begins to decelerate while approaching the target, it is now desirable for the robot to apply positive damping. As positive damping is applied to the system, the human user can focus on stabilizing within the target.

For the robot to transition from negative to positive damping while the user performs a target reaching task, the robot requires a quantification of the "user intent." Based on the previous description of a human user performing a target reaching task, the acceleration is a good candidate for quantifying user intent since its sign represents the intent of the user to start and stop motion. However, this quantification can be improved by taking the product of the velocity ($\dot{x}$) and acceleration vectors ($\ddot{x}$), which then represents a scaled version of the change in kinetic energy and therefore has a more desirable physical meaning.

Rather than instantaneously switching from a maximum negative robotic damping condition to a maximum positive robotic damping condition, the variable damping controller is defined by a piecewise logistic function to smoothly transition between the positive and negative damping (Eq. (1)). A piecewise function was selected to allow the designer to set the robotic damping, b_C, when the user intent is zero regardless of the positive and negative damping limits, b_{UB} and b_{LB}, which are not generally of equal magnitude.

$$B(\dot{x}\ddot{x}) = \begin{cases} \dfrac{2b_{LB}}{1+e^{-k_p\dot{x}\ddot{x}}} - b_{LB} + b_C, & \dot{x}\ddot{x} \geq 0 \\ -\dfrac{2b_{UB}}{1+e^{-k_n\dot{x}\ddot{x}}} + b_{UB} + b_C, & \dot{x}\ddot{x} < 0 \end{cases} \quad (1)$$

where B is the robotic damping applied in 1-DOF and $b_{LB} + b_C$ and $b_{UB} + b_C$ are the lower and upper asymptotes of the damping range. In addition to the user intent $\dot{x}\ddot{x}$, tuning constants k_p and k_n are used as they described in (2) to specify the logistic growth rate of the function, which determines how quickly to transition between $b_{LB} + b_C$ and $b_{UB} + b_C$.

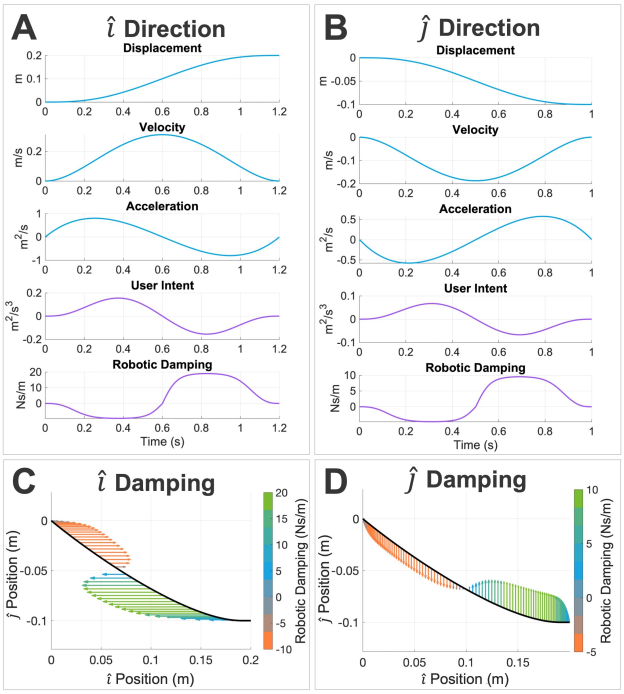

Fig. 1. Simulation results of the variable damping controller in 2-DOF. **A-B:** Simulation results using minimum jerk trajectory as an input to the variable damping controller. By tuning the controller based on the extrema of the user intent, the robotic damping plot shows the use of the full range of damping in both the $\hat{\imath}$ and $\hat{\jmath}$ directions. **C-D**: A 2D trajectory plot in black showing the damping applied in each direction, with a color range used to show the different magnitudes and directions of robotic damping applied by the variable damping controller. Negative damping is shown in orange, positive damping in green.

$$k_p = \frac{-ln\left(\frac{1-s}{1+s}\right)}{\dot{x}\ddot{x}_{max}}, \qquad k_n = \frac{-ln\left(\frac{1+s}{1-s}\right)}{\dot{x}\ddot{x}_{min}} \tag{2}$$

where $\dot{x}\ddot{x}_{max}$ and $\dot{x}\ddot{x}_{min}$ are the maximum and minimum user intent during typical movement of the extremity and s represents the desired sensitivity of the robotic damping function. In this study, $s = 0.95$, which means that the robotic damping will be $0.95b_{LB} + b_C$ at $\dot{x}\ddot{x}_{max}$ and $0.95b_{UB} + b_C$ at $\dot{x}\ddot{x}_{min}$. Therefore, k_p and k_n can be selected such that the robotic damping will transition through the full range of damping, $[b_{LB}+b_C, b_{UB}+b_C]$.

In the two experiments simulating the industrial and rehabilitation applications of the proposed variable damping controller, there are multiple DOFs that must be considered simultaneously. For a human arm performing a target reaching task in a horizontally planar workspace—analogous to the types of tasks common in industrial applications—there are two translational directions of motion that must be considered: the medial-lateral (ML) and antero-posterior (AP) directions. Similarly, for a human ankle performing a target reaching task—analogous to the types of tasks common in many rehabilitation applications—there are two rotational directions of interest: the inversion-eversion (IE) and dorsiflexion-plantarflexion (DP) directions. Though the upper-extremity/industrial application considers translational motion and the lower-extremity/rehabilitation application considers rotational motion, both cases can be addressed using a 2-DOF implementation of the variable damping controller.

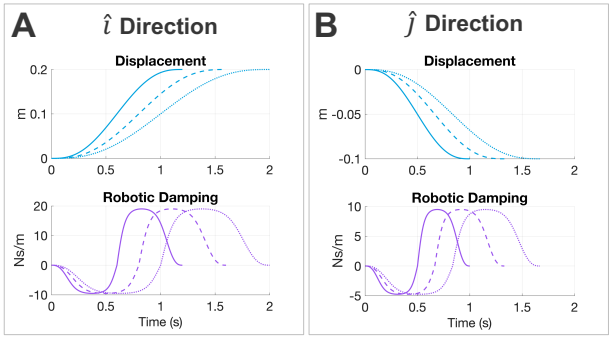

Fig. 2. Simulation results in 2-DOF that demonstrate that the tuning of the controller allows different human users to move at different speeds while still experiencing the full damping range of the controller. The solid lines represent the same simulation as performed in Fig. 1, while the dashed and dotted lines simulated slower movement.

In both the upper- and lower-extremity implementations of the controller, one of the first considerations is the inherent human joint/limb damping with which the robot is interacting. Since different DOFs of parts of the human body have different inherent damping, the controller is designed so that the variable damping control is decoupled for each DOF. Therefore, the ML and AP directions of the upper-extremity planar motion are considered separately by the controller, and likewise for the IE and DP directions of the ankle (Eq. (3)). Note that $\hat{\imath}$ and $\hat{\jmath}$ are unit vectors specifying the direction of planar motion (in the upper-extremity case) and rotational motion (in the lower-extremity case).

$$\boldsymbol{B_r} = \begin{cases} B_{ML}\hat{\imath} + B_{AP}\hat{\jmath} & \textit{upper-extremity} \\ B_{IE}\hat{\imath} + B_{DP}\hat{\jmath} & \textit{lower-extremity} \end{cases} \tag{3}$$

B. Simulations

To ensure the effectiveness of the controller, two simulations were performed. The first simulation focused on the use of user intent, $\dot{x}\ddot{x}_{max}$ and $\dot{x}\ddot{x}_{min}$, to calculate the tuning constants, k_p and k_n, and output of the robotic damping response, $\boldsymbol{B_r}$. For this simulation, two position profiles needed to be generated to simulate the movement of the human user in the $\hat{\imath}$ and $\hat{\jmath}$ directions. Using a minimum jerk trajectory function (Eq. (4)), these positions could be simulated as smooth paths from a starting position to an ending (target) position.

$$x = x_{target}\left[10\left(\frac{t}{t_d}\right)^3 - 15\left(\frac{t}{t_d}\right)^4 + 6\left(\frac{t}{t_d}\right)^5\right] \tag{4}$$

where x_{target} represents the target position of the human user and t_d represents the duration of motion. For the simulation, the initial position was set at (0, 0) and the target was set at a position of (0.2, -0.1). Slightly different durations of movement were set for the $\hat{\imath}$ and $\hat{\jmath}$ directions, with the movement in the $\hat{\imath}$ direction taking 0.2 s longer than movement in the $\hat{\jmath}$ direction. Damping ranges of [-10, 20] Ns/m ($\hat{\imath}$ direction) and [-5, 10] Ns/m ($\hat{\jmath}$ direction) with $b_C = 0$ were selected for the simulation.

The simulation shows the kinematic and damping responses for both DOFs (Fig. 1). With the equation for minimum jerk

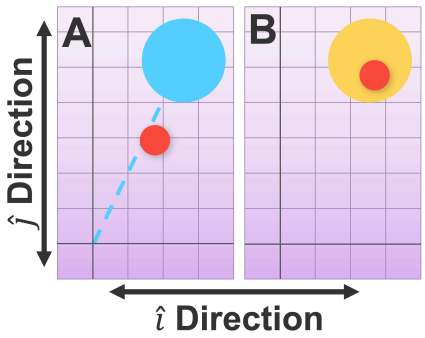

Fig. 3. GUI used for target reaching experiment. **A:** Cursor signified by a red circle; targets signified by blue circles. A blue dashed line represented the straightest path between the previous target and the next. **B:** Once a user reached the target position, the target became orange as a visual indication that they were inside the target.

trajectory and calculating the time derivatives to find velocity and acceleration, the kinematic response was defined. Taking the product of the velocity and acceleration responses yields the quantification of user intent. In this simulation, the minimum and maximum values from the user intent plot were used to calculate the tuning constants for the calculation of the variable damping response. In both the $\hat{\imath}$ and $\hat{\jmath}$ directions, the full damping range was used.

A second simulation was performed to ensure that the variable damping controller could be tuned for human users that move at different speeds (Fig. 2). Using the same parameters as used in the first simulation, the original duration of time to complete the task (1.2 s in $\hat{\imath}$ direction and 1.0 s in $\hat{\jmath}$ direction) was increased by 33.3% (1.6 s in $\hat{\imath}$ direction and 1.3 s in $\hat{\jmath}$ direction) and 66.7% (2.0 s in $\hat{\imath}$ direction and 1.7 s in $\hat{\jmath}$ direction) to simulate three different users who take different amounts of time to complete the task. Without tuning the controller to each user, some users might not use the full range of robotic damping, since the controller would not be able to anticipate the typical values of $\dot{x}\ddot{x}_{max}$ and $\dot{x}\ddot{x}_{min}$. The simulation demonstrates that the controller can be tuned to the typical kinematic response of each user.

III. Methods for Experimental Validation

A. Experimental Protocol

Human experiments were performed to evaluate the variable damping controller. Two experiments were performed with 20 healthy subjects each which implemented the variable damping controller: 1) in an upper-extremity experiment and 2) in a lower-extremity experiment. Both experiments required subjects to complete a series of point-to-point target reaching tasks while coupled to a robot. While the different robotic hardware and ranges of motion for the two experiments necessitates some small differences in the experimental protocols, the two experiments shared many common procedures, which will be described in this section, and the following two sections will discuss the specific differences between the two experimental protocols. The goal of performing two separate experiments was to demonstrate the general applicability of the controller for different parts of the human body.

To instruct the subjects where to move throughout the experiment, a GUI was created that showed the subject their current position within the robot's workspace, to where they should move, (Fig. 3A) and whether they were successfully within the target position (Fig. 3B). This visual feedback was placed approximately ~1 m from the subject (Fig. 4 B and D).

The structure of the experiment was defined by a collection of trials, movements of a subject from one target position to the next, and blocks, a set of ten trials. The full study consisted of a total of 220 trials, separated into 22 blocks between which subjects were given a one-minute break to rest. The first six blocks were used for tuning the two DOFs of the variable damping controllers separately, the next two blocks were used for practice, and the final 14 blocks, called the main blocks, were those used for the data analysis. The instructions for all the blocks were the same: each time a target appears on the screen, move as fast as possible to the target while avoiding overshoot. In the practice and main blocks, the subjects interacted with a variable damping condition and a constant positive damping condition. The constant positive damping condition was chosen as an experimental control condition, with the magnitude of positive damping selected to be a small value that prevented large overshoots.

For each trial within the six tuning blocks, subjects were required to move from a neutral position, along either the $\hat{\imath}$ or $\hat{\jmath}$ directions, and then move back to the neutral position. Since the $\hat{\imath}$ and $\hat{\jmath}$ controllers are independent of one another, they were tuned separately, with three consecutive blocks for tuning the $\hat{\imath}$ controller and three more for tuning the $\hat{\jmath}$ controller. Within each set of three blocks, the first block calculated the tuning constants while applying zero robotic damping, the second block used the tuning constants calculated in the first block to apply variable damping while calculating a new set of tuning constants, and the third block repeated the same process as the second block to calculate the final tuning constants used for all the later variable damping blocks. By the end of the six tuning blocks, four tuning constants had been found: $k_p^{\hat{\imath}}$, $k_p^{\hat{\jmath}}$, $k_n^{\hat{\imath}}$, and $k_n^{\hat{\jmath}}$, where the superscript identifies the DOF corresponding to the tuning constant.

Following the six tuning blocks were two practice blocks, which introduced the subject to the 2D target reaching task. During these practice blocks and all the later main blocks, targets would appear within the defined workspace centered at the neutral position. A trial was considered complete when the subject stabilized within the target for two consecutive seconds. Within the practice blocks, there was one block where the robot was applying constant positive damping in both directions and one block where the robot was applying variable damping in both directions. Subjects were not informed that there were different damping environments between blocks.

After the two practice blocks, the subject continued to the 14 main blocks. The main blocks were indistinguishable from practice blocks from the perspective of the subject. However, instead of alternating between positive and variable damping each block as was done for the two practice blocks, the 14 main blocks were grouped together so that the subjects had time to acclimate to the different damping conditions. The blocks were grouped in two sets of three blocks, followed by two sets of four blocks. Within each set of blocks, the damping environment

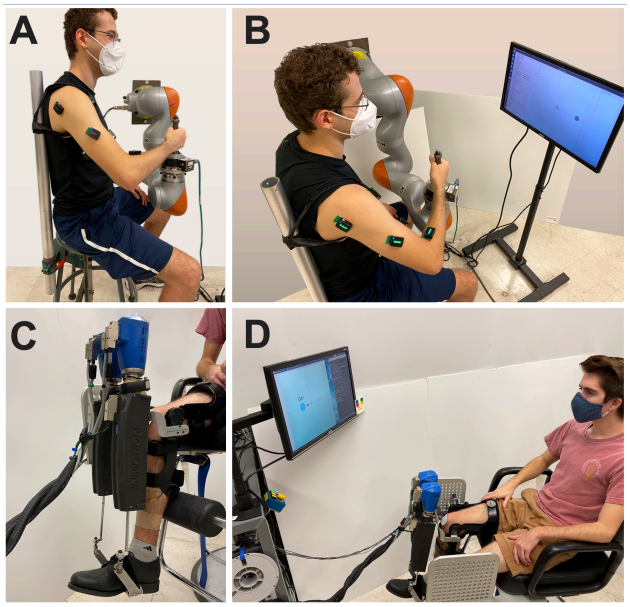

Fig. 4. Experimental setups to evaluate the effectiveness of the variable damping controller. **A-B**: Human user holding the end-effector of the 7-DOF robotic arm for the upper-extremity experiment. **C-D**: Human user coupled to the wearable ankle robot for the lower-extremity experiment.

alternated, and the order that these damping environments were shown in the experiment was randomized between subjects.

In total, the 22 blocks and one-minute breaks between each block took less than one hour, ensuring that the subjects did not become fatigued throughout the study. The targets were placed in such a way that they did not favor either the $\hat{\imath}$ or $\hat{\jmath}$ directions.

1) Upper-Extremity Experiment: For the upper-extremity experiment, the variable damping controller was implemented into a 7-DOF robotic arm (LBR iiwa R820, KUKA, Germany) with a 6-axis load cell (Delta IP60, ATI Industrial Automation, NC) attached to the end-effector, where the human user would grasp while moving their dominant arm in the ML ($\hat{\imath}$) and AP ($\hat{\jmath}$) directions. Because of the addition of the 6-axis load cell, force data could be collected during the experiment, in addition to kinematic and muscle activation data. Kinematic and force data was sampled at 1 kHz.

A total of 20 young, healthy subjects (age: 20–33, weight: 48–100 kg, 4 female, 16 male) participated in this study, which was approved by the Institutional Review Board of Arizona State University (STUDY00008114). All subjects gave written consent prior to participation and were not aware of the study's hypothesis. Each of the subjects completed the experimental protocol in a seated position while holding the end-effector of the robot (Fig 4A). The subjects could move the end effector in only the ML and AP directions (the transverse plane of motion), as the stiffness of the end effector was set to 0 N/m in these directions, and 10^6 N/m in the perpendicular direction. In addition to the 0 N/m stiffness in the transverse plane, the inertia was set to 10 kg. The subjects were seated with a neutral position defined as holding the robot with the elbow at 90° of flexion and shoulder at 70° of abduction and 45° of horizontal flexion. Subjects were instructed to hold their wrist at a constant neural position and not allow any relative angle change between the hand and forearm. The stool the subjects were seated on was positioned to allow movement of 18 cm in any of the four directions ($+\hat{\imath}$, $-\hat{\imath}$, $+\hat{\jmath}$, and $-\hat{\jmath}$) along the transverse plane. For the safety of the human user, a virtual wall of size 36 cm by 36 cm was created around the workspace, so any movement at or outside of that perimeter would be prevented by imposing a highly positive damping of 30 Ns/m.

Within both the practice and main blocks, the ten targets were placed in such a way that the overall path length within a block was 50 cm in each of the four movement directions (medial, lateral, anterior, and posterior) and the minimum displacement in each direction in each trial was more than 5 cm. A path was generated in the plane with dimension of 20×20 cm^2 around the neutral position. Target sizes had the radius of 1.5 cm, while the radius of the cursor for subject position was 5 mm. The following damping ranges were selected based on upper-extremity characterization studies [24, 25]: [-10, 60] Ns/m for the ML direction and [-30, 60] Ns/m for the AP direction. In-between trials the damping was set to 30 Ns/m for safety purposes. During the tuning blocks, each trial required a motion of ±10 cm in each direction.

Electromyography (EMG) data was recorded by surface EMG sensors (Trigno Wireless EMG System, DELSYS Inc., USA) placed on the dominant arm of the subject. All subjects that participated in the experiment were right-handed. The muscles recorded were the brachioradialis (BRD), biceps (BI), anterior deltoid ($DELT_{ANT}$), posterior deltoid ($DELT_{POST}$), and the lateral and longitudinal triceps (TRI_{LAT} and TRI_{LONG}). All sites of application were thoroughly cleaned with alcohol pads before placing the sensors. Sensors were secured with double-sided adhesive tape and waterproof skin tape. After attaching the sensors, the subject was instructed to perform a maximum voluntary contraction (MVC) test for each of the muscles following standard muscle testing procedures [29, 30]. This involved three repetitions of an isokinetic movement for each muscle. There was a three second hold for each repetition and a one second rest in-between repetitions. All MVC movements occurred while the subject was standing, and all EMG data for the upper-extremity experiment was sampled at 2 kHz.

2) Lower-Extremity Experiment: For the lower-extremity experiment, the variable damping controller was implemented into a wearable ankle robot (Anklebot, Bionik Laboratories Corp., Canada). The wearable robot is highly backdrivable and could therefore apply damping in the IE ($\hat{\imath}$) and DP ($\hat{\jmath}$) directions of the human's ankle as they moved. There is no force sensor on this robot, so no interaction force data was collected throughout the experiment.

A total of 20 young, healthy subjects (age: 21–34, weight: 48–91 kg, 7 female, 13 male) participated in this study, which was approved by the Institutional Review Board of Arizona State University (STUDY00012606). All subjects gave written consent prior to participation and were not aware of the study's hypothesis.

The wearable ankle robot was supported by a knee brace and connected to the human subject with joints on the subject's right shoe (Fig. 4B). All subjects wore the same style of rigid shoe with a flat sole. The robot was then calibrated to a neutral foot position of 90° from the shank in the DP direction to the sole of the shoe. Afterwards, gravity compensation was performed so that a constant, upwards torque was applied throughout the

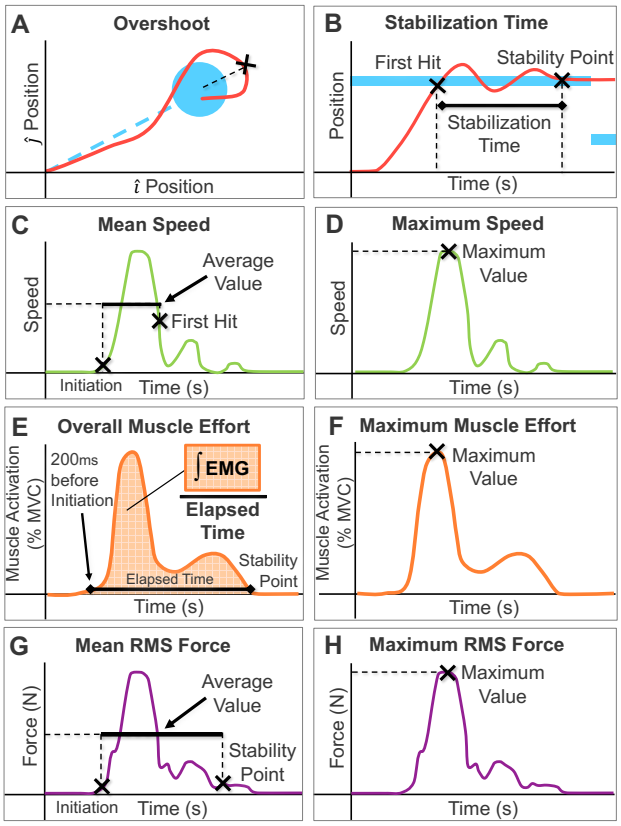

Fig. 5. Visual representations of the performance metrics selected for data analysis. Row 1 shows stability metrics, with the target position in blue and position response in red. Row 2 shows the agility metrics in green. Rows 3 and 4 show the effort metrics, with muscle activation in orange and force in violet. The illustration of muscle activation could be considered as the contribution from a single muscle or the average of multiple agonists.

study to prevent fatigue. Before the main portion of the experiment, the subjects performed the tuning trials. During the tuning trials, subjects had to move ±7.5° in the IE direction and ±15° (for the first set of three tuning blocks) in the DP direction (for the second set of three tuning blocks) and then return to the neutral position.

The targets for the practice and main portion of the experiment (blocks 7–22) were placed on the end of randomly generated path segments within an ellipse that was ±15° tall and ±7.5° wide. These values were chosen to remain within the documented range of motion for the human ankle [31]. All paths for each block were selected to have the same amount of distance traveled in the DP and IE directions within ±1°. The total path length for all trials within a block was 55±1°. The targets had a radius of 2.5°, and the user's cursor had a radius of 0.75°.

EMG data was recorded by surface EMG sensors (Bagnoli-16, DELSYS Inc., USA) placed on the tibialis anterior (TA), peroneus longus (PL), medial gastrocnemius (MG), and soleus (SL), and a grounding sensor was placed on the subject's kneecap. Procedures for EMG setting and MVC measurement were the same as in the upper-extremity experiment.

B. Data Analysis

To analyze the data collected during the 14 main blocks in the experimental protocol, a number of performance metrics were selected. These performance metrics convert the raw kinematic, EMG, and interaction force (upper-extremity experiment only) data into meaningful quantities that are used to represent the effectiveness of the controller. Selecting the point-to-point target reaching task for both experiments allowed for the presentation of variety of performance metrics that are minimally task specific. Since the goal of the variable damping controller is to improve the trade-off between stability/agility and reduce user effort in pHRI, there are three main categories of performance metrics in this paper: stability, agility, and user effort.

1) Stability: Stability was quantified by evaluating the amount of overshoot and the time required to stabilize in each trial. A stable trial was defined as one in which the subject moved along a straight path to the target without going past the target. If the subject passed the target along the ideal line from the previous target to the next, the maximum tangential distance from the target along the ideal line was quantified as the overshoot (Fig 5A). Additionally, the time period during which this overshoot was taking place (between when the subject first hit the target to the stability point) was quantified as the stabilization time (Fig. 5B). The stability point was defined as the time when the subject was able to hold the center of the cursor within the target for 0.5 s.

2) Agility: Agility was quantified by evaluating the speed at which subjects completed each trial. Two separate metrics of speed were evaluated: mean speed and maximum speed. The mean speed was calculated during the main portion of the trial from when the subject started moving, the initiation time, to when they first hit the target, the first hit time. The initiation time was quantified as the point in time when the subject moved at least 5 mm (in the upper-extremity experiment) or 2° (in the lower-extremity experiment) in any direction around their initial position. The first hit was quantified as the point in time when the subject hit the outer edge of the target with the cursor. Between these two times, the mean speed was calculated for each trial (Fig. 5C). The second agility metric was the maximum speed, which was simply a quantification of the largest magnitude speed achieved by a subject during each trial (Fig 5D).

3) User Effort: User effort was quantified in both experiments by the muscle activation and, in the upper-extremity experiment, by force at the interaction point. Muscle activation data was collected by surface EMG sensors on the muscles relevant to motion. All EMG data, including that of the MVC, was filtered using a 4th order low-pass Butterworth filter with a frequency of 5 Hz after removing the DC bias offsets and rectifying the signal. All EMG data was normalized by the MVC value for each muscle. This was calculated by taking the average of 1 second's worth of data surrounding the maximum data point from the MVC test. A single peak data point was not chosen because it would allow too much variability [32].

The two metrics to evaluate the EMG data were overall effort and maximum effort. The overall effort was defined as the integral of the processed EMG curve from 200 ms before the

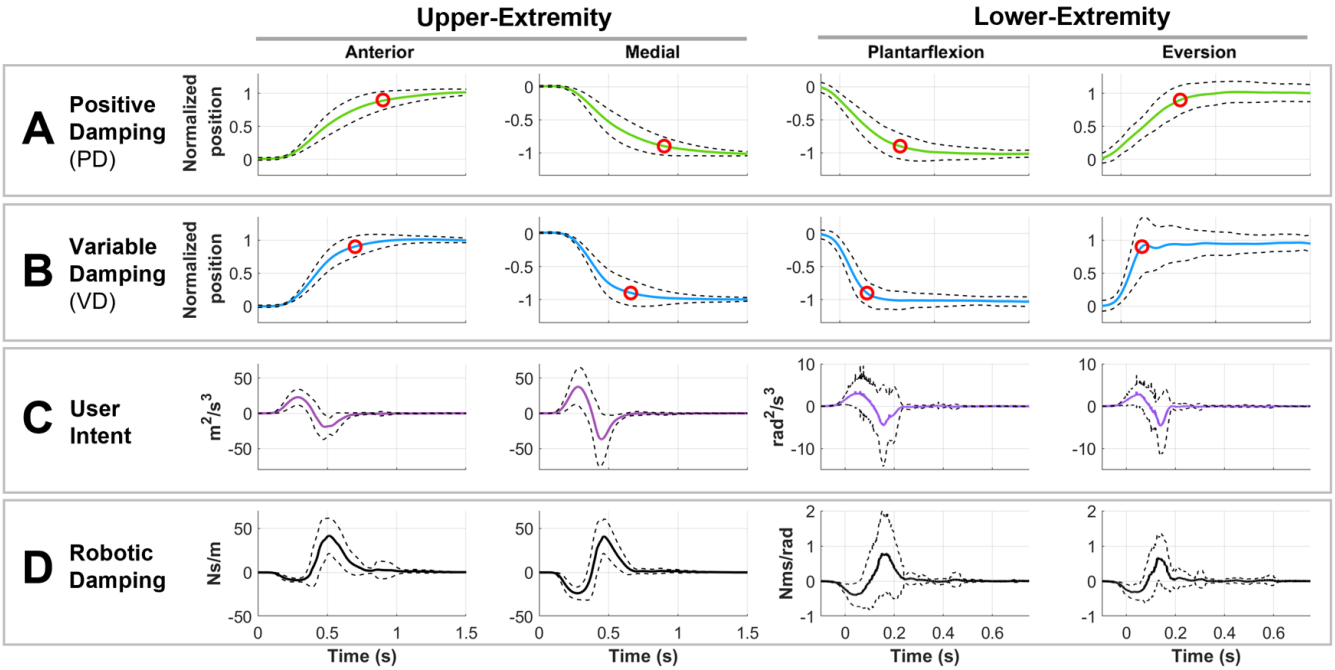

Fig. 6. A representative subject's kinematic data. The two leftmost columns represent the data of the anterior and medial direction from the upper-extremity study, while the last two columns are the dorsiflexion and eversion data from the lower-extremity study. The position data in the first two rows (**A**: positive, **B**: variable) are displayed as normalized values to account for the differences in path lengths, with the starting location indicated with a normalized position of 0 and a target location with a normalized position of ±1. User intent is shown in **C** and the average variable damping applied across the trials is shown in **D**. The dotted lines represent ±1 STD from the mean.

initiation time to the stability point (Fig 5E). The 200 ms of EMG data before the initiation time was included to capture the muscle activation required to initiate movement. This value was then divided by the time elapsed over when the integral was taken, and then averaged with the values calculated for the agonists of the appropriate direction of movement. The relevant agonist muscles for each direction were as follows. For the upper-extremity study: forward corresponded to the TRI_{LONG} and TRI_{LAT}, backwards to the BRD and BI, left to the TRI_{LAT}, TRI_{LONG}, and $DELT_{ANT}$, and right to the $DELT_{POST}$, BRD, and BI. For the lower extremity study: dorsiflexion corresponded to the TA, plantarflexion to the SL and MG, and eversion to the PL. Inversion motion was not quantifiable using surface EMG sensors and thus was not considered. The maximum effort metric was calculated by taking the maximum value of activation over the whole trial and averaging it with the other agonists, similar to the overall effort (Fig. 5F).

In addition, the mean root-mean-squared (RMS) and maximum RMS interaction force were used in the upper-extremity experiment to quantify kinetic reduction in effort. The mean RMS interaction force was taken from the initiation time to the stability point (Fig. 5G). The maximum interaction force was simply the highest value of interaction force over the course of the whole trial (Fig. 5H).

4) Additional Considerations and Statistical Analysis: Outlier rejection was applied to all performance metrics using the normalized position response in each movement direction. The trials were shifted to align the position response, and any trial that fell outside of ±3 standard deviations (STD) from the mean position response was removed.

Statistical analysis was performed to assess the significance of mean differences between the variable and positive damping conditions. Two-tailed, paired t-tests were used for all kinematic metrics and non-paired t-tests were used for all EMG metrics. This is because both EMG metrics are reported with the variable condition as a ratio to the positive such that the t-test is comparing normalized variable damping data to one with an unknown variance. All statistical tests used a significance level of 0.05.

IV. Results

Results from the 20 subjects in both the upper- and lower-extremity studies confirmed that the variable damping controller was able to reduce user effort while simultaneously improving agility with a minimal reduction in stability. The subsections below describe the results from a representative subject and the group results from each study. To be concise, variable damping and positive damping are abbreviated as VD and PD, respectively, within this section. The average percent of trials removed per subject from the upper-extremity experiment were 4.9 ± 1.5% and 6.1 ± 1.5% for PD and VD respectively. Similarly, for the lower-extremity experiment, averages of 5.5 ± 1.3% (PD) and 7.7 ± 2.1% (VD) of trials were removed as outliers.

A. Representative Subject Results

The position profiles for the representative subject (Fig. 6A and 6B) were shifted in time and normalized so that the initiation of movement (time when the subject had moved 5 mm for the upper-extremity study and 2° for the lower-extremity study) is represented as a position of zero and the target is a

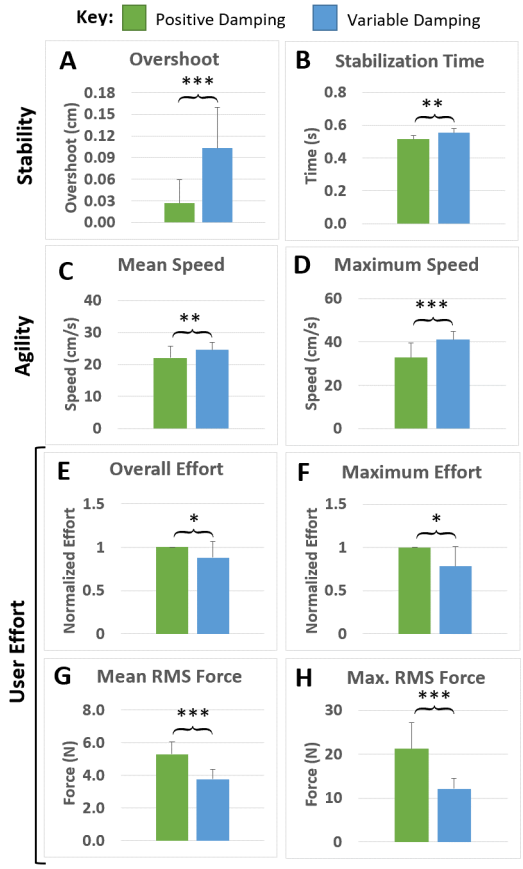

Fig. 7. The group-averaged results for the kinematic and EMG data of the upper-extremity study. Group averages are represented by the height of the bars. The error bars show a range of ±1 standard deviation from the mean. Stars are used to denote significance in pairwise comparisons: ** for $p < 0.001$, and *** for $p < 1E\text{-}4$.

position of ±1. Both the upper- and lower-extremity position profiles with the VD controller show a low amount of overshoot, and the difference in overshoot between the two damping conditions is almost negligible. This shows that the ability of VD to provide a level of stability comparable to PD. Marked in red hollow circles, the mean time to reach 90% of the normalized target position occurs sooner in the VD condition than the PD condition. This result demonstrates the increased agility with the VD controller.

Further, the effectiveness of the VD controller can be seen in the representative subject results of user intent and robotic damping. These results show how the damping applied (Fig. 6D) is dependent on the user intent (Fig. 6C). Positive user intent causes negative damping which helps the user accelerate, while negative user intent causes positive damping which allows users to stabilize within the target position. Fig. 6C shows how quickly the VD controller was able to assist with acceleration and deceleration over the course of the trial.

B. Group Results: Upper-Extremity Study

1) Stability: The overshoot and stabilization time metrics provided a means for comparing the impact each controller has on the stability of the user (Fig 7A and 7B). Neither the PD nor VD condition caused a significant amount of overshoot (≤ 0.1 cm). This result is in comparison to the minimum and maximum

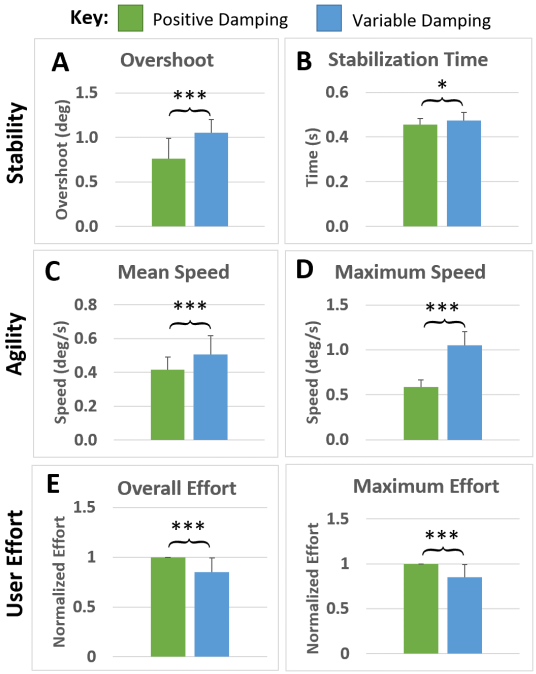

Fig. 8. The group-averaged results for the kinematic and EMG data of the lower-extremity study. The error bars show a range of ±1 standard deviation from the mean. Stars are used to denote significance in pairwise comparisons: * for $p < 0.05$ ** for $p < 0.001$, and *** for $p < 1E\text{-}4$.

path lengths of 7 cm and 28 cm, respectively. The overshoot was 0.07 cm greater for VD than PD. While a paired t-test demonstrated a significant difference ($p < 1E\text{-}4$) in overshoot between the damping conditions, the small magnitude of the VD overshoot (< 2% of the minimum possible path length) overall is inconsequential. The second stability metric, stabilization time, had a 7.5% increase in time required to reach the target after movement initiation. This result represents a difference in means of 0.04 s and is statistically significant according to a paired t-test ($p < 1E\text{-}4$). However, as with the overshoot metric results, this difference is largely inconsequential.

2) Agility: The agility metrics show that the VD controller allowed subjects to move more quickly than the PD controller. VD produced faster mean and maximum speeds than those of PD (Fig. 7C and 7D). The mean speed of VD was 2.5 cm/s higher than PD representing a 10.7% increase, while the maximum speed of VD was 8.1 cm/s higher than PD representing a 22.2% increase. Both results were found to be statistically significant using a paired t-test ($p < 0.001$, $p < 1E\text{-}4$ for mean and maximum speed, respectively).

3) User Effort: User effort was quantified using two metrics, muscle effort and interaction force. The muscle effort metrics demonstrate the biomechanical reduction in effort as a function of muscle activation, while the interaction force metrics are an outward representation of the muscle effort. Intersubject variability in the MVC caused by differences in muscle size was reduced by normalizing VD to PD. The overall muscle effort metric (Fig. 7E) showed a 11.9% decrease in muscle activation, while the maximum muscle effort metric (Fig. 7F) showed a 21.8% decrease. A t-test comparing the normalized value of VD to one showed that both the overall and maximum muscle effort

had a statistically significant difference in mean values ($p < 0.001$ and $p < 1E-4$, respectively).

Both the mean and maximum RMS force applied in VD were significantly lower than PD (Fig. 7G and 7H). The mean RMS force in VD was 1.5 N less than PD representing a 33.9% decrease, while the maximum RMS force in VD was 9.2 N less than PD, representing a 54.9% decrease. These results were found to be statistically significant using a paired t-test ($p < 1E-4$ for both mean and maximum RMS force), demonstrating a kinetic reduction in effort associated with the VD controller.

C. Group Results: Lower-Extremity Study

1) Stability: There was a significant difference ($p < 1E-4$) in overshoot between the means of the two damping conditions (Fig. 8A) as reported by a paired t-test. This represented a 28.2% increase in overshoot from PD to VD and an increase in mean of 0.25°. Despite this significant difference in means, the overshoot in both conditions was very small (< ~1°), relative to a minimum and maximum path lengths of 4.1° and 15.4°, respectively. The stabilization time metric (Fig. 8B) also had a significant difference ($p < 0.005$) between the two damping conditions as reported by a paired t-test. There was a 2.2% difference between conditions representing a 0.01 s difference in the average time it took subjects to stabilize. Although statistically significant, this difference is not large enough to indicate a substantial reduction in the user's stability.

2) Agility: The agility metrics demonstrate that subjects were able to maneuver at statistically significantly higher speeds in VD compared to PD ($p < 1E-4$ for both metrics). This significance was determined using a paired t-test for both metrics. There was an increase in mean speed (Fig. 8C) of 19.4% corresponding to a mean difference of 0.09 cm/s from PD to VD. There was also an increase in maximum speed (Fig. 8D) by 56.1% representing a difference in means of 0.46 cm/s. These metrics demonstrate a statistically significant increase in agility effected by the VD controller.

3) User Effort: The muscle effort metrics demonstrate that the subjects were able to perform the tasks with significantly less effort using the VD controller than the PD controller. The overall and maximum effort metrics show respective 15.2% and 15.3% decreases in required agonist muscle activation from PD to VD (Fig. 8E and F). A t-test comparing the normalized value of VD to one showed denoted a significant difference in means for both metrics ($p < 1E-4$ for both overall and maximum muscle effort).

V. Discussion

Impedance/admittance controllers with constant positive damping have been widely used in many pHRI applications due to the importance of stability in coupled human robot systems. However, these control methods over-emphasize stability at the expense of agility and user effort. In this study, the variable damping controller was developed on the principle of using both positive and negative damping to provide a solution that balances stability, agility and user effort.

Our previous work in variable damping control was limited to 1D applications [27, 28]. This allowed us to establish a proof of concept for our methodology; however, 1D movement is not an accurate representation of tasks encountered in everyday life. This 2D study is meant to fill this gap and more closely represent the behavior of the controller in real-world scenarios.

The results of both the upper- and lower-extremity studies demonstrate that the variable damping controller was able to reduce user effort while increasing agility at a negligible cost to stability. The reduction in user effort has significant implications for long-term use where the user may not possess the stamina required to operate a less efficient coupled human-robot system. The implementations of the VD controller described in this work may be directly applied to rehabilitation where the use of lower- [33] and upper-extremity [34] movements for reaching tasks are common. Industrial applications may also benefit from the efficiency of the VD controller to mitigate the development of musculoskeletal diseases that develop as a result of strenuous labor [35]. While the amount of translational benefit of this controller in weight-bearing pHRI has not yet been quantified, previous research has shown that improved motor control in non-weight bearing training can be transferred to weight-bearing daily tasks [33, 36]. In general, the improvement in agility allows the user to have a more seamless experience during pHRI that is not limited by the dissipative energy dynamics caused by a positive damping controller [37]. Nearly equivalent stability in damping conditions shows that the variable damping controller effectively emulates desired deceleration dynamics of positive damping. Increased agility and positive damping stability demonstrate that the variable damping controller combines the useful elements of both negative and positive damping to develop a more efficient control mechanism.

Existing works on variable impedance/admittance controllers in pHRI have improved the performance of coupled human-robot systems. However, the performance of these controllers was evaluated with limited or task-specific metrics such as reducing force measured at the interaction point [23], reducing time completion of a specific task [17, 19, 20], or reducing oscillation while maintaining a specific amount of force [21]. Unlike previous work, this paper evaluated several categories of metrics to demonstrate the performance of the proposed controller from a more holistic view in two separate applications. The proposed controller could maintain stability, increase agility, and reduce user effort, in both the upper- and lower-extremities. All three of these characteristics are essential in the design of coupled human-robot systems.

While the current implementation of the variable damping controller was shown to successfully manage the trade-off between stability, agility, and user effort in multi-DOF, it still requires tuning and many static parameters. Several tuning trials must be completed to ensure each subject's maximum and minimum user intent are paired with the respective values of damping. Furthermore, the maximum and minimum values of damping simulated by the controller were determined from the results of the previous characterization studies [24–26]. Therefore, while these values are chosen based on knowledge from the biomechanical characteristics of the average human user, they are not based on biomechanical characteristics of

each individual user. A more robust method would be to have these parameters continually update as user proficiency improves. However, the impact of user proficiency is not currently factored into the design of the controller. The current study was implemented using only the point-to-point target reaching task. This task allowed us to present many different, general performance parameters and to show the generality of our method. Although more complicated tasks such as irregular movement and obstacle avoidance are not directly studied, the point-to-point target reaching task serves as an important building block for such movements.

Future work will focus on developing learning methods so that the controller can adaptively tune its parameters based on the performance and biomechanical characteristics of each user. This would eliminate the tuning sessions and incorporate the ability and proficiency of each user. Other future work will focus on integrating additional biomechanical characteristics of humans, like stiffness, into the design variable impedance controllers. The validated, improved controller may then be tested using irregular movement tasks.

REFERENCES

[1] H. Krebs, and B. Volpe, "Rehabilitation robotics," in *Handbook of clinical neurology*, vol. 110, pp. 283–294, 2013.

[2] P. Morasso, M. Casadio, V. Sanguineti, V. Squeri and E. Vergaro, "Robot therapy: the importance of haptic interaction," *2007 Virtual Rehabilitation*, Venice, Italy, 2007, pp. 70-77.

[3] C. Heyer, "Human-robot interaction and future industrial robotics applications," *2010 IEEE/RSJ Int. Conf. Intelligent Robots and Sys.*, Taipei, 2010, pp. 4749-4754.

[4] C. Loughlin, A. Albu-Schäffer, S. Haddadin, C. Ott, A. Stemmer, T. Wimböck, and G. Hirzinger, "The DLR lightweight robot: design and control concepts for robots in human environments," *Industrial Robot: int. j.*, vol. 34, no. 5, pp. 376-385, Aug. 2007.

[5] A. B. Zoss, H. Kazerooni and A. Chu, "Biomechanical design of the Berkeley lower extremity exoskeleton (BLEEX)," in *IEEE/ASME Trans. Mechatronics*, vol. 11, no. 2, pp. 128-138, Apr. 2006.

[6] S. Chiaverini, B. Siciliano, and L. Villani, "A survey of robot interaction control schemes with experimental comparison," in *IEEE/ASME Trans. Mechatronics*, vol. 4, no. 3, pp. 273–285, 1999.

[7] S. G. Khan, G. Herrmann, M. Al Grafi, T. Pipe, and C. Melhuish, "Compliance control and human–robot interaction: Part 1—survey," in *Int. J. Humanoid Robotics*, vol. 11, no. 03, p.1430001, 2014.

[8] A. Calanca, R. Muradore, and P. Fiorini, "A review of algorithms for compliant control of stiff and fixed-compliance robots," in *IEEE/ASME Trans. Mechatronics*, vol. 21, no. 2, pp. 613–624, 2015.

[9] E. Colgate, N. Hogan, "The Interaction of Robots with Passive Environments: Application to Force Feedback Control," in *Waldron K.J. (eds) Advanced Robotics: 1989*. Springer, Berlin, Heidelberg.

[10] N. Hogan, "Impedance Control: An Approach to Manipulation," *1984 American Control Conf.*, San Diego, CA, USA, 1984, pp. 304-313.

[11] W. S. Newman, "Stability and Performance Limits of Interaction Controllers," ASME. *J. Dyn. Sys., Meas., Control*, vol. 114 no. 4, pp. 563–570, Dec. 1992.

[12] S.P. Buerger, and N. Hogan, "Impedance and interaction control," in T.R. Kurfess (Ed.), *Robotics and automation handbook*, Boca Raton, FL: CRC Press, 2004, pp. 368-391.

[13] A. Albu-Schäffer, C. Ott, and G. Hirzinger, "A unified passivity-based control framework for position, torque and impedance control of flexible joint robots," *The Int. J. Robotics Research*, vol. 26, no. 1, pp. 23–39, 2007.

[14] B. Hannaford and Jee-Hwan Ryu, "Time-domain passivity control of haptic interfaces," in *IEEE Trans. Robotics and Automation*, vol. 18, no. 1, pp. 1-10, Feb. 2002.

[15] C. Ott, A. Albu-Schaffer, A. Kugi and G. Hirzinger, "On the Passivity-Based Impedance Control of Flexible Joint Robots," in *IEEE Trans. Robotics*, vol. 24, no. 2, pp. 416-429, Apr. 2008.

[16] H. Lee and N. Hogan, "Essential considerations for design and control of human-interactive robots," *2016 IEEE Int. Conf. Robotics and Automation (ICRA)*, Stockholm, 2016, pp. 3069-3074.

[17] K. H. Lee, S. G. Baek, H. J. Lee, H. R. Choi, H. Moon and J. C. Koo, "Improving transparency in physical human-robot interaction using an impedance compensator," *2017 IEEE/RSJ Int. Conf. Intelligent Robots and Sys. (IROS)*, Vancouver, BC, 2017, pp. 3591-3596.

[18] F. Ferraguti, C. Talignani Landi, L. Sabattini, M. Bonf˙e, C. Fantuzzi, and C. Secchi, "A variable admittance control strategy for stable physical human–robot interaction," *The Int. J. Robotics Research*, vol. 38, no. 6, pp. 747–765, 2019.

[19] R. Ikeura and H. Inooka, "Variable impedance control of a robot for cooperation with a human," *Proc. 1995 IEEE Int. Conf. on Robotics and Automation*, Nagoya, Japan, 1995, pp. 3097-3102 vol.3,

[20] V. Duchaine and C. M. Gosselin, "General Model of Human-Robot Cooperation Using a Novel Velocity Based Variable Impedance Control," *2nd Joint EuroHaptics Conf. and Symp. on Haptic Interfaces for Virtual Environ. and Teleoperator Systems (WHC'07)*, Tsukaba, 2007, pp. 446-451.

[21] H. Li *et al*., "Stable and Compliant Motion of Physical Human–Robot Interaction Coupled with a Moving Environment Using Variable Admittance and Adaptive Control," in *IEEE Robotics and Automation Letters*, vol. 3, no. 3, pp. 2493-2500, July 2018

[22] C. T. Landi, F. Ferraguti, L. Sabattini, C. Secchi and C. Fantuzzi, "Admittance control parameter adaptation for physical human-robot interaction," *2017 IEEE Int. Conf. on Robotics and Automation (ICRA)*, Singapore, 2017, pp. 2911-2916.

[23] H. Li, T. Nuradha, S. A. Xavier and U. Tan, "Towards A Compliant and Accurate Cooperative Micromanipulator using Variable Admittance Control," *2018 3rd Int. Conf. on Advanced Robotics and Mechatronics (ICARM)*, Singapore, 2018, pp. 230-235.

[24] F. Zahedi, T. Bitz, C. Phillips, and H. Lee, "Regulation of 2d arm stability against unstable, damping-defined environments in physical human-robot interaction," in *IEEE/RSJ International Conference on Intelligent Robots and Systems (IROS)*, 2020.

[25] F. Zahedi and H. Lee, "Human arm stability in relation to damping-defined mechanical environments in physical interaction with a robotic arm," Submitted in *Int. Conf. on Robotics and Automation* (ICRA), 2021.

[26] H. Lee, H. I. Krebs and N. Hogan, "Multivariable Dynamic Ankle Mechanical Impedance with Active Muscles," in *IEEE Transactions on Neural Systems and Rehabilitation Engineering*, vol. 22, no. 5, pp. 971-981, Sept. 2014.

[27] J. Arnold, H. Hanzlick and H. Lee, "Variable Damping Control of the Robotic Ankle Joint to Improve Trade-off between Performance and Stability," *2019 Int. Conf. on Robotics and Automation (ICRA)*, Montreal, QC, Canada, 2019, pp. 1699-1704.

[28] T. Bitz, F. Zahedi and H. Lee, "Variable Damping Control of a Robotic Arm to Improve Trade-off between Agility and Stability and Reduce User Effort," *2020 IEEE Int. Conf. on Robotics and Automation (ICRA)*, Paris, France, 2020, pp. 11259-11265.

[29] J. Montgomery, and D. Avers. "Daniels and Worthingham's Muscle Testing: Techniques of Manual Examination" (8th ed.). Philadelphia: Saunders, 2007.

[30] E. Criswell , "Cram's Introduction to Surface Electromyography," (2nd ed.) Sudbury: Jones and Bartlett, 2011. ch. 17.

[31] C. L. Brockett, G. J. Chapman, "Biomechanics of the ankle," *Journal of Orthopaedic Trauma*, 2016, vol. 30, no. 3, pp. 232-238.

[32] P. Konrad, "The ABC of EMG: A Practical Introduction to Kinesiological Electromyography," Scottsdale: Noraxon, 2005, pp. 31

[33] L. W. Forrester, A. Roy, H. Krebs, R. Macho, "Ankle training with a robotic device improves hemiparetic gait after a stroke," *Neurorehabil. Neural Repair*, vol. 25, pp. 369–377, 2011.

[34] G. Kwakkel, J. B. Kollen, and H. I. Krebs. "Effects of robot-assisted therapy on upper limb recovery after stroke: a systematic review." *Neurorehabil. Neural Repair*, 2008, vol. 22, no. 2, pp. 111-121.

[35] C. C. for O. H. and S. Government of Canada, "Work-related Musculoskeletal Disorders (WMSDs); OSH Answers," *Canadian Centre for Occupation of Health and Safety,* January, 2013, [Online], Available: https://www.ccohs.ca/oshanswers/diseases/rmirsi.html. [Accessed: 14-Jan-2021].

[36] J. L. Chang, R.Y. Lin, M. Saul, P. J. Koch, H. Krebs, and B. T. Volpe, "Intensive seated robotic training of the ankle in patients with chronic stroke differentially improves gait," *NeuroRehabilitation*, 2017, vol. 4, pp. 61-68.

[37] K. Tokuda, B. Lee, Y. Shiihara, K. Takahashi, N. Wada, K. Shirakura, and H. Watanabe, "Muscle activation patterns in acceleration-based phases during reach-to-grasp movement," *Journal of Physical Therapy Science*, 2016, vol. 28, no. 11, pp. 3105–3111

Fatemeh Zahedi received the B.Sc. degree in electrical engineering from Shiraz University, Shiraz, Iran, in 2015 and the M.Sc. degree in electrical engineering from Sharif University of Technology, Tehran, Iran in 2017. She is currently pursuing the Ph.D. degree in mechanical engineering at Arizona State University, Tempe, USA.

Since 2018, she has been a Research Associate with the Neuromuscular Control and Human Robotics Laboratory with the school of Matter, Transport, and Energy, Arizona State University. Her research interests include physical human-robot interaction, control systems, rehabilitation robotics, and machine learning.

James Arnold received a B.S.E. degree in mechanical engineering and a M.S. degree in robotics and autonomous systems from Arizona State University, Tempe, Arizona, USA in 2019 and 2021, respectively. He will be pursuing a Ph.D. degree in mechanical engineering at Harvard University, Cambridge, Massachusetts, USA starting in the fall of 2021.

He is currently a software engineering intern at the MathWorks, Natick, Massachusetts, USA. His research interests include physical human-robot interaction, control systems, and machine learning.

Connor Phillips is pursuing a B.S.E degree in mechanical engineering at Arizona State University, Tempe, Arizona, United States. He will graduate in December 2021.

He is currently interning at the National Institutes of Health (NIH), Bethesda, Maryland and will be pursuing a Postbaccalaureate IRTA fellowship at the NIH following his graduation. His research interests include physical human-robot interaction, electroencephalography, and the rehabilitation of neuromuscular disorders.

Hyunglae Lee (M' 13) is an Associate Professor of Mechanical and Aerospace Engineering at Arizona State University, Tempe, Arizona, United States, where he directs the Neuromuscular Control and Human Robotics Laboratory. He received his Ph.D in Mechanical Engineering from Massachusetts Institute of Technology (MIT) and worked as a postdoctoral fellow at the Sensory Motor Performance Program, Rehabilitation Institute of Chicago (RIC; now ShirleyRyan AbilityLab). His current research interest includes physical human robot interaction, rehabilitation robotics, and neuromotor control. He is a recipient of NSF CAREER Award (2019), Top 5% Teaching Award at ASU Ira A. Fulton Schools of Engineering (2019-20, 2020-21), Winner of the Innovation Challenge in WearRAcon (1st place in 2020 and 2nd place in 2021), Outstanding Paper Award in International Conference on Ubiquitous Robots (2018), Sarah Baskin Award (2014), Finalist for the Best Student Paper Award in IEEE BioRob (2012), Samsung Scholarship (2008-2013), and Top Graduation Award (ranked 1st in class 2002) in the School of Mechanical and Aerospace Engineering at SNU (2002).